Numerical Examinations of the Stability of FDTD Subgridding Schemes

Shumin Wang

Laboratory of Functional and Molecular Imaging, National Institute of Neurological Disorders and Stroke, National Institutes of Health
10 Center Dr., 10/B1D728, Bethesda, MD 20892, U. S. A.
E-mail: james.wang@ieee.org

Abstract **–** The stability of two-dimensional Finite-Difference Time-Domain subgridding schemes was numerically examined. Both the same-time-step and the multiple-time-step schemes were considered. Results show that the multiple-time-step subgridding scheme is late-time unstable due to larger-than-unity eigenvalues. As to the same-time-step subgridding schemes, stability is related to the treatment of corner regions.

Keywords **–** FDTD method, subgridding, stability.

I. INTRODUCTION

Since the Finite-Difference Time-Domain (FDTD) method was introduced [1],[2], a major challenge is modeling locally fine structures and/or field singularities. To model fine features or resolve rapid field variations, small cells are required and the overall computational cost can be prohibitive by using the traditional FDTD method.

One attractive solution is subgridding, i.e., fine meshes are employed wherever needed and the rest of the computational domain is discretized by coarse meshes. The early version of subgridding applies the FDTD method twice in different regions, where the results in coarse region are used as boundary conditions for fine regions [3]. Due to the lack of timely feedback from fine regions, this approach only yields better results in fine regions. To improve the accuracy, fine regions are embedded into coarse regions and the timely feedback is provided by field coupling on boundaries [4]. In this scheme, two methods are possible to accommodate the stability requirement imposed by fine region cell size. One is to use the same time step (STS) size, which is dictated by the fine region cell size, in both regions. The other is to use different time step sizes determined by coarse and fine region cell sizes respectively. Thus one time step in coarse region corresponds to multiple time steps (MTS) in fine region. Accordingly, temporal interpolation is required for field coupling on the boundaries.

Despite the various accuracy-enhancement procedures [5]-[8], FDTD subgridding methods are notorious for their late-time instability, which typically happens after many iterations. To address this issue, spatial reciprocity on coarse-fine region boundaries has proposed as a necessary condition to achieve late-time stability [9]. However, its effectiveness remains unclear. In this paper, we provide numerical examinations of its sufficiency for both the STS and the MTS subgridding schemes.

The dominant eigenvalues of the system amplification matrices are examined as a key measure of stability. Meanwhile, corresponding numerical simulations are carried out for sufficient time steps to check the actual late-time behavior. For simplicity, 2D *TEz* wave was examined. The subgridding refinement ratio is 3:1. The odd ratio results in collocated coarse-fine region boundary values in space and in time. For other subgridding ratios, the analysis follows the same procedure. We note that the main purpose of this paper is to provide first-hand numerical examinations. Theoretical explanations are given tentatively based on known theories.

This paper is organized as follows. Section II presents the methodology and describes the numerical tests. Section III verifies the approach by the regular FDTD scheme. Sections IV and V show the results of the STS and the MTS schemes, respectively. Finally, conclusion remarks are drawn in section VI.

II. METHODOLOGY

The stability of FDTD subgridding schemes was first studied by the dominant eigenvalues of the system amplification matrices [2]. In the discretized Maxwell's equations

$$\begin{pmatrix} \vec{E}^{\,n} \\ \vec{H}^{\,n+1/2} \end{pmatrix} = [A] \cdot \begin{pmatrix} \vec{E}^{\,n-1} \\ \vec{H}^{\,n-1/2} \end{pmatrix}, \tag{1}$$

[A] denotes the system amplification matrix. To verify the late-time behavior, simulations were carried out inside Perfect Electric Conducting (PEC) boxes of various sizes. A magnetic point source near the lower-left corner was excited and the electric field at another location was monitored at each time step. The source is a differentiated Gaussian pulse and its peak

magnitude is less than one. Therefore, the observed electrical field magnitude should not be larger than one in a stable simulation. Whenever the above condition is violated, we claim that a simulation is unstable and that time step is recorded as the "critical point". Otherwise, the most recent observations were checked after ten million time steps. If they do not show any sign of growth, a scheme is claimed as numerically stable.

The fine region is placed at the center of the computational domain, which is denoted by $m \times n$, where m is the distance from the fine region boundary to the outer boundary of the entire computational domain and n the size of the fine region, both are in terms of the coarse region cell size.

We note that the maximum possible value at the observation is different with respect to different computational domain sizes. The "critical point" only indicates instability and its value should not be interpreted in the same way for different computational domains. Due of limited resources, we only considered small computational domains. However, stability is usually characterized asymptotically by assuming an infinitely large one. To examine the differences and verify our approach, we first study the regular FDTD method.

III. THE REGULAR FDTD METHOD

Figure 1 shows the dominant eigenvalues of the system amplification matrix of the regular FDTD method as a function of the Courant-Friedrichs-Levy (CFL) number, which is defined by $\Delta t\sqrt{2}v_p / \Delta h$. Here, v_p is the phase velocity, Δh is the cell size and Δt is the time-step size. The computational domain size is denoted by $m \times n$ in terms of cells, where m represents the length and n represents the width.

It is interesting to notice that simulations of very small computational domains can be stable even with a larger than one CFL number. For a 3 × 3 PEC box, the largest stable CFL number reaches to 1.15 (the CFL numbers are resolved to 0.01 in this article). As the computational domain size increases, the largest stable CFL number drops rapidly and becomes one when the computational domain size is equal to or larger than 12 × 12. These results were confirmed by simulations.

The above observations can be understood by the asymptotic nature of theoretical stability analysis, which only considers the worst case in the Von Neumman analysis [2]. It is well known that the time step size of 2D FDTD simulations is restricted by

$$\Delta t \le \frac{h}{v_p\sqrt{\sin^2\left(\frac{k_x h}{2}\right)+\sin^2\left(\frac{k_y h}{2}\right)}} \qquad (2)$$

where k_x and k_y are associated with the discrete Fourier modes [10] and the worst case is $k_x h = k_y h = (2n+1)\pi$. In an infinitely large computational domain, there are infinite Fourier modes including the above worst case. When the computational domain size is limited, the discrete Fourier modes that can possibly exist are limited and they may not include the worst case. The stability condition determined directly by the dominant eigenvalues of small computational domains can be different from that of the Von Neumman analysis. Therefore, multiple tests with increasing computational domain sizes are suggested to estimate the asymptotic behavior of numerical stability.

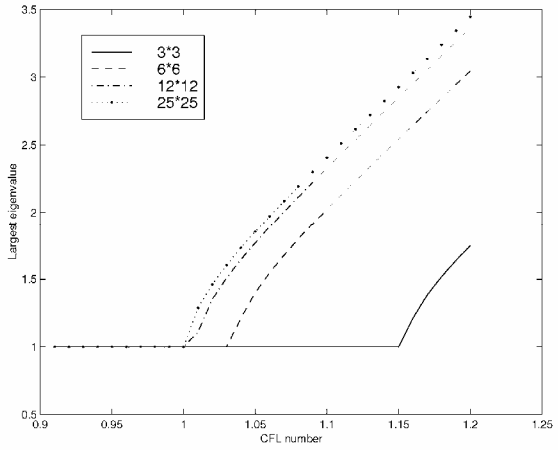

Fig. 1. Dominant eigenvalues of the system amplification matrix of the regular 2D FDTD method according to different CFL numbers and computational domain sizes.

IV. THE STS SUBGRIDDING SCHEME

In general, we can write the STS scheme as

$$\begin{pmatrix} \vec{U}^{\,n+1/2} \\ \vec{u}^{\,n+1/2} \end{pmatrix} = \begin{pmatrix} A_{CC} & A_{CF} \\ A_{FC} & A_{FF} \end{pmatrix} \cdot \begin{pmatrix} \vec{U}^{\,n-1/2} \\ \vec{u}^{\,n-1/2} \end{pmatrix} \qquad (3)$$

where $\vec{U}^{\,n+1/2}$ contains all coarse region unknowns and $\vec{u}^{\,n+1/2}$ contains all fine region unknowns, both at the current time step. A_{CC} represents how the coarse region uses the previous coarse region values, A_{CF} represents how the coarse region uses the previous fine region values, A_{FC} represents how the fine region uses the previous coarse region values and A_{FF} represents how the fine region uses the previous fine region values.

Figures 2 and 3 depict a regular coarse-fine region boundary and a corner region respectively. In order to calculate the fine region boundary electric field, e.g. e_{y1}, we need the coarse region magnetic field, e.g. h'_{z1}. To

recover the missing values due to boundary truncation, the following linear interpolation is employed [8],

$$h'_{z1} = \frac{2}{3}H_{z1} + \frac{1}{3}H_{z2} \ , \tag{4}$$

$$h'_{z2} = \frac{1}{3}H_{z1} + \frac{2}{3}H_{z2} \ , \tag{5}$$

$$h'_{z3} = H_{z2} . \tag{6}$$

Instead of being half-cell away from the boundary electric field, the recovered magnetic field is 1.5-cell away. To keep at least first-order accuracy in space, we employed the unbalanced differencing scheme to update the boundary electric field, e.g.,

$$e^{n}_{y1} = e^{n-1}_{y1} + \frac{\Delta t}{2\Delta h\varepsilon}\left(h'^{\,n-1/2}_{z1} - h^{n-1/2}_{z1}\right) \tag{7}$$

where Δh is the fine region cell size. When calculating the coarse region boundary magnetic field, e.g. H_{z2}, we need the electric field along the coarse-fine region boundary, e.g. E_{y2}. They are obtained by enforcing spatial reciprocity [9], i.e.,

$$E_{y2} = \frac{1}{3}\left[\frac{1}{3}\left(e_{y1} + e_{y5}\right) + \frac{2}{3}\left(e_{y2} + e_{y4}\right) + e_{y3}\right]. \tag{8}$$

Note that the coarse region boundary magnetic field is calculated by central differencing scheme in the layout shown in Fig. 2. Another choice is to extend the fine region 1/3 coarse cell (or one fine cell) to the left, i.e., overlapping the coarse and fine regions by one fine cell. In that case, the coarse region boundary magnetic field is calculated by unbalanced differencing and the fine region boundary electric field is calculated by central differencing. Since unbalanced differencing scheme is first-order accurate, choosing fine region boundary electric field to be calculated by unbalanced differencing scheme is apparently more accurate.

As we shall see, the real difficulty is to treat corners, e.g., h'_{z1} and in h''_{z1} Fig. 3, by imposing spatial reciprocity. If we write

$$h'_{z1} = \frac{2}{3}H_{z1} + \frac{1}{3}H_{z3}, h''_{z1} = \frac{2}{3}H_{z2} + \frac{1}{3}H_{z3}, \tag{9}$$

the coarse region boundary electrical field can be obtained by spatial reciprocity as,

$$E_{x3} = E_{x3} + \frac{1}{9}e_{x1}, E_{y3} = E_{y3} + \frac{1}{9}e_{y1} . \tag{10}$$

This apparently introduces errors when calculating H_{z3} (also H_{z1} and in H_{z2}). To improve the accuracy, other corner layouts can be applied by shifting the fine region boundary field components and violating the reciprocity. Since spatial reciprocity is our major concern, we employ the layout shown in Fig. 3 and refer to it as "reciprocal with corner" treatment.

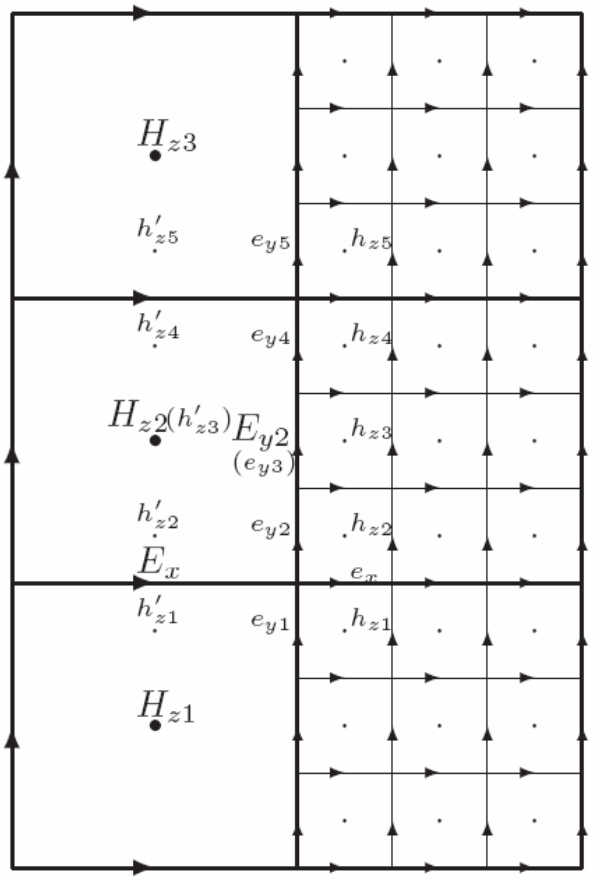

Fig. 2. The coarse-fine region boundary.

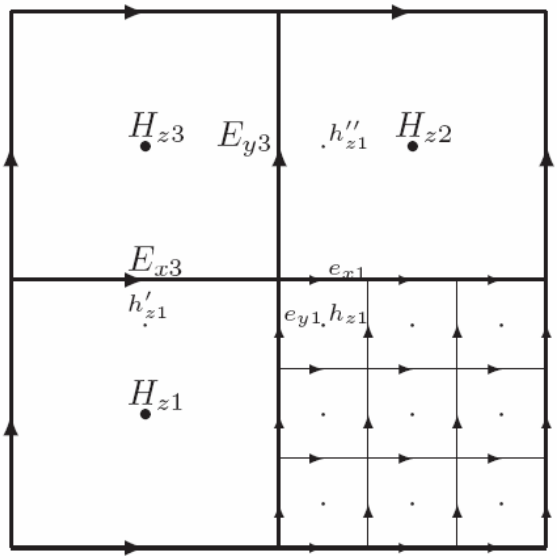

Fig. 3. The coarse-fine region boundary at a corner.

Alternatively, one may simply ignore corners and write

$$h'_{z1} = H_{z1}, h''_{z1} = H_{z2} . \tag{11}$$

This can be physically interpreted as treating H_{z1} and H_{z2} as the average in those cells. In the following, we refer to

this as "reciprocal without corner" treatment.

A. Reciprocal with Corner

An example of the system amplification matrix is illustrated in Fig. 4, which corresponds to a "3 × 3" subgridding region. The dominant eigenvalue of this example is 1.420754 when the CFL number is 1.03. As we decrease the CFL number, the dominant eigenvalue drops quickly and becomes 1.0 when the CFL number is 1.01. We further calculated the dominant eigenvalues of subgridding schemes with larger computational domain sizes (up to "10 × 10"). It was found that the results are all 1.0 when the CFL number is 1.0.

Although the dominant eigenvalues do not show any sign of instability for CFL=1, numerical simulations were unstable for all computational domains being tested. Moreover, the instability does not happen late. For example, the "3 × 3" case became unstable after 360 time steps. The "9 ×10" case is the most stable one, which only runs stably for 3689 time steps. This example shows that enforcing spatial reciprocity on coarse-fine region boundaries is not a sufficient condition for stability in general.

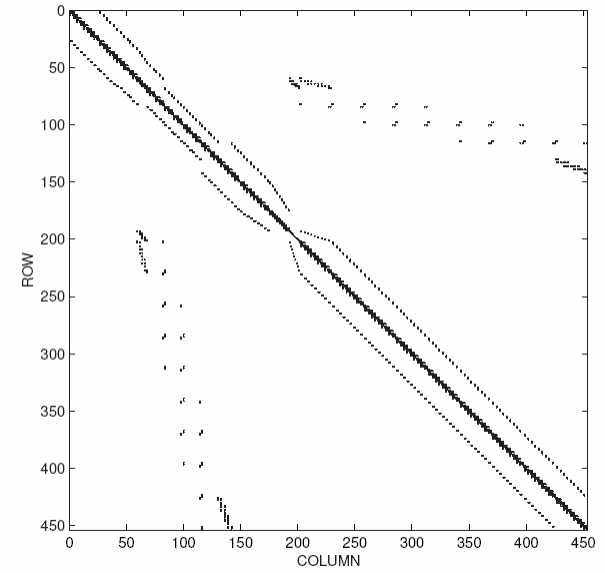

Fig. 4. An example of the system amplification matrix of the "reciprocal with corner" treatment.

B. Reciprocal without Corner

The same set of subgridding layout was examined. The system amplification matrices look similar to Fig. 4. The dominant eigenvalue of the "3 × 3" case is 1.420752 when the CFL number is 1.03. As we decrease the CFL number, the dominant eigenvalue drops quickly and becomes 1.0 when the CFL number is 1.01. For subgridding schemes with larger computational domain sizes (up to "10 ×10") the dominant eigenvalues are all 1.0 when the CFL numbers are 1.0.

Contrary to the previous case, numerical simulations were stable with ten million time steps for all computational domains being tested.

V. THE MTS SUBGRIDDING SCHEME

The major difference between the STS and the MTS subgridding schemes is the timing procedure involved in the latter case. Figure 5 illustrates the case where one coarse-region time-step corresponds to three fine-region time-steps. When calculating e^n and $e^{n+1/3}$ in fine region, we need $H^{n-1/6}$ and $H^{n+1/6}$ in coarse region for spatial interpolation. Also, when calculating $H^{n+1/2}$ by imposing reciprocity, we need e^n in fine region. These two requirements make accurate temporal interpolation, i.e., obtaining $H^{n-1/6}$ and $H^{n+1/6}$ by $H^{n-1/2}$ and $H^{n+1/2}$, difficult to implement if special reciprocity has to be enforced. One solution is to use temporal extrapolation, i.e., obtaining $H^{n-1/6}$ and $H^{n+1/6}$ by $H^{n-1/2}$ and $H^{n-3/2}$, etc. Alternatively, one may also use $H^{n-1/2}$ for $H^{n-1/6}$ and $H^{n+1/6}$ [9], which is frequently referred to as Zeroth Order Hold (ZOH) in digital signal processing [11]. ZOH inevitably introduces spectrum distortion to input signals. However, we chose ZOH because temporal extrapolation is more prone to instability in practice.

The implementation of the above timing procedure results in the following set of equations,

$$\vec{u}^{\,n-1/6} = A_{FF}\vec{u}^{\,n-1/2} + A_{FC}\vec{U}^{\,n-1/2}, \tag{12}$$

$$\vec{u}^{\,n+1/6} = A_{FF}^2\vec{u}^{\,n-1/2} + \left(A_{FF}+1\right)\cdot A_{FC}\vec{U}^{\,n-1/2}, \tag{13}$$

$$\vec{u}^{\,n+1/2} = A_{FF}^3\vec{u}^{\,n-1/2} + \left(A_{FF}^2 + A_{FF}+1\right)\cdot A_{FC}\vec{U}^{\,n-1/2}, \tag{14}$$

$$\begin{aligned}\vec{U}^{\,n+1/2} &= A_{CC}\vec{U}^{\,n-1/2} + A_{CF}\vec{u}^{\,n-1/6} \\ &= \left(A_{CC} + A_{CF}\cdot A_{FC}\right)\vec{U}^{\,n-1/2} \\ &\quad + A_{CF}\cdot A_{FF}\vec{u}^{\,n-1/2}\end{aligned} \tag{15}$$

where all symbols have the same meaning as in equation (3). Accordingly, the system amplification matrix is written as

$$A = \begin{bmatrix} A_{CC} + A_{CF}\cdot A_{FC} & A_{CF}\cdot A_{FF} \\ \left(A_{FF}^2 + A_{FF}+1\right)\cdot A_{FC} & A_{FF}^3 \end{bmatrix}. \tag{16}$$

Figure 6 illustrates the amplification matrix of the "3 × 3" case. Figure 7 shows the dominant eigenvalues vs. the CFL numbers for different sizes of computational domain and subgridding region. As we see, the dominant eigenvalues are always larger than 1.0 regardless of the CFL number. As the size of computational domain increases, the dominant eigenvalue for a given CFL

number decreases but never reaches 1.0. Numerical simulations further verified the above results, where the recorded "critical points" are shown in Fig. 8. These results correspond to the dominant eigenvalues in Fig. 7 well.

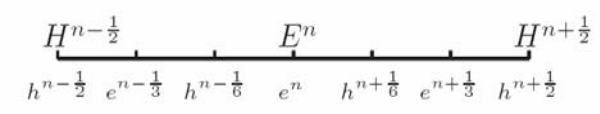

Fig. 5. Timing of the MTS subgridding scheme, where superscripts denote the time-step.

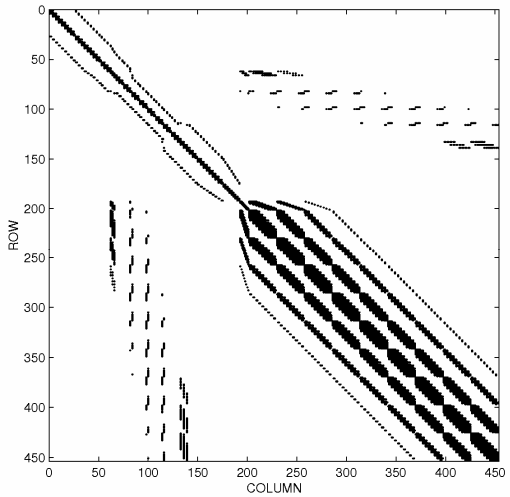

Fig. 6. An example of the system amplification matrix of the MTS subgridding scheme.

The MTS scheme is more efficient than the STS scheme. As demonstrated in Fig. 7, the dominant eigenvalues decrease with either an increasing computational domain size or a decreasing CFL number. Thus in practice, one may delay the late-time instability by either decreasing the CFL number or by increasing the computational domain size.

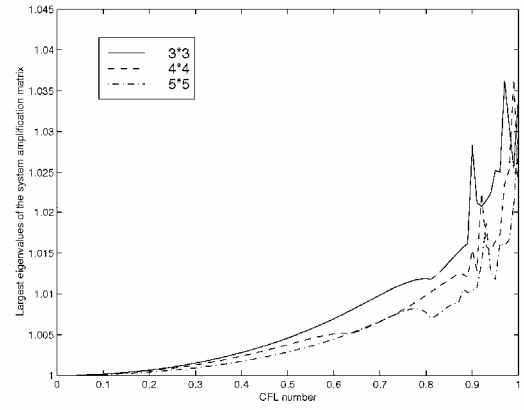

Fig. 7. Dominant eigenvalues of the MTS subgridding scheme.

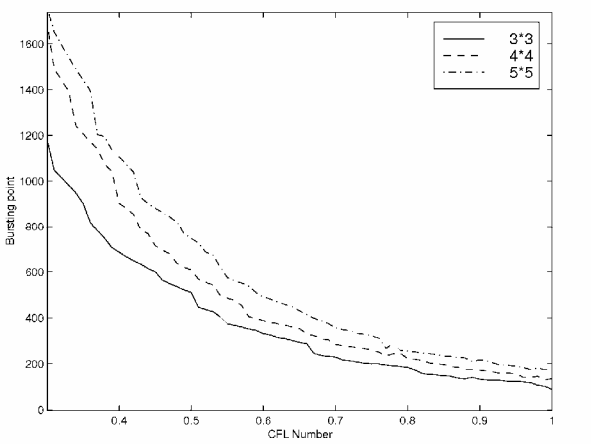

Fig. 8. "Critical points" of the MTS subgridding scheme with different computational domain sizes and different CFL numbers.

VI. CONCLUSIONS

We numerically examined the stability of both the STS and the MTS FDTD subgridding schemes. For the STS schemes, it was shown that enforcing spatial reciprocity does not guarantee stability in general, especially when corners must be handled in a reciprocal manner. As to the MTS subgridding schemes, the system is unstable due to eigenvalues that are out of the unit circle. Some practical considerations were also given with regard to the use of FDTD subgridding schemes. Future work involves developing stable FDTD subgridding schemes.

REFERENCES

[1] K. S. Yee, "Numerical solution of initial boundary value problems involving Maxwell's equation in isotropic media," *IEEE Trans. Antennas Propag*., vol. 14, no. 3, pp. 302-307, 1966.

[2] A. Taflove *Advances in computational electrodynamics: the finite-difference time-domain method*, Artech: Boston.

[3] K. S. Kunz and L. Simpson, "A technique for increasing the resolution of finite-difference solution of the Maxwell equation," *IEEE Trans. Electromagn. Compat*., vol. 23, no. 4, pp.419-422, 1981.

[4] I. S. Kim and W. J. R. Hoefer *A local mesh refinement for the time-domain finite-difference method using Maxwell's curl equations*, IEEE Trans. Microwave Theory Tech. 1990; 38(6):812-815.

[5] S. S. Zivanovic, K. S. Yee, and K. K. Mei, "A subgridding method for the time-domain finite-difference method to solve Maxwell's equations," *IEEE Trans. Microwave Theory Tech*.,

vol. 39, no. 3, pp. 471-479, 1991.

[6] M. Okoniewski, E. Okoniewski, and M. A. Stuchly, "Three-dimensional subgridding algorithm for FDTD," *IEEE Trans. Antennas Propag.*, vol. 45, no. 3, pp. 422-429, 1997.

[7] M. W. Chevalier, R. J. Luebbers, and V. P. Cable, "FDTD local grid with material transverse," *IEEE Trans. Antennas Propag*., vol. 45, no. 3, pp. 411-421, 1997.

[8] S. Wang, F. L. Teixeira, R. Lee, and J-F. Lee, "Optimization of subgridding schemes for FDTD," *IEEE Microwave and Wireless Components Lett*., vol. 12, no. 6, pp. 223-225, 2002.

[9] P. Thoma and T. Weiland, "A consistent subgridding scheme for the finite difference time domain method," *International Journal of Numerical Modeling: Electronic Network, Devices and Fields*, vol. 9, no. 5, pp. 359-374, 1996.

[10] J. W. Thomas *Numerical Partial Differential Equations: Finite Difference Methods*. Springer Verlag: New York.

[11] B. Porat *A course in digital signal processing*. John Wiley & Sons: New York.

Shumin Wang received the B.S. degree in physics from Qingdao University, and the M.S. degree in electronics from Peking University, China, in 1995 and 1998, respectively, and the Ph.D. degree in electrical engineering from The Ohio State University, Columbus, Ohio, in 2003. He is a Staff Scientist at the National Institutes of Health, Bethesda, Maryland. His research interests include time-domain differential equation based methods, integral equation methods, high frequency asymptotic methods and their applications to bio-medical and electromagnetic scattering problems.